

# Investigation on Crack Tip Transformation in NiTi Alloys: Effect of the Temperature

Emanuele Sgambitterra<sup>1</sup> · Carmine Maletta<sup>1</sup> · Franco Furgiuele<sup>1</sup>

Published online: 5 June 2015  
© ASM International 2015

**Abstract** The effect of the temperature on crack tip transformation in Nickel–Titanium (NiTi) shape memory alloys was analyzed in this work by means of experimental and analytical approaches. In particular, single edge crack specimens were analyzed for two different values of the testing temperature in the pseudoelastic regime of the alloy, i.e.,  $T = 298$  K and  $T = 338$  K. The thermal-dependent phase transition mechanisms occurring at the crack tip region were studied by analyzing data obtained from digital image correlation as well as by nanoindentation experiments performed near the crack tip. Finally, experimental results were compared with predictions of a recent analytical model. Results revealed that an increase in temperature causes a decrease of the phase transformation zone and that both the techniques are well suitable in capturing the thermal effect on the phase transformation mechanisms near the crack tip.

**Keywords** Shape memory · NiTi alloys · Stress-induced martensitic transformation · Fracture · Nanoindentation · Digital image correlation

## Introduction

Nickel–Titanium-based (NiTi) shape memory alloys (SMAs) have seen increasing interest in the last few years, from both engineering and scientific communities, due to

their special functional properties, namely shape memory effect (SME) and pseudoelastic effect (PE) [1, 2]. These properties are due to a reversible solid state phase transition between a parent phase (austenite) and a product phase (martensite), the so-called thermoelastic martensitic transformation (TMT) [2], that can be activated either by temperature (thermally induced martensite, TIM), or by applied stress (stress-induced martensite, SIM). Due to these unique features, NiTi alloys are currently used in an increasing number of engineering applications [3], where both SME and PE are used for the realization of smart components and systems. However, thanks to their good mechanical properties and biocompatibility, the most important applications of NiTi alloys are in the field of medicine [4], where pseudoelasticity is mainly exploited for the realization of several components, such as cardiovascular stent, embolic protection filters, orthopedic components, orthodontic wires, micro surgical, and endoscopic devices. As a direct consequence of this increasing interest, several experimental studies were carried out in the last decades, to better understand the thermo-mechanical properties of NiTi alloys [2]. However, many aspects are still unknown, especially because the hysteretic stress and/or thermally induced phase transformations significantly affect the damage mechanisms occurring under fatigue loadings, i.e., the crack formation and propagation mechanisms. In fact, the fracture behavior of austenitic NiTi alloys strongly depends on the SIM transformation occurring near the crack tip region, as a consequence of the high values of local stresses. As a direct consequence of the marked non-linear and hysteretic behavior, classic elastic and/or elastic–plastic theories cannot be directly applied to SMAs.

In this context, both the fatigue crack propagation [5–12] and the fracture properties under static loadings

---

✉ Emanuele Sgambitterra  
emanuele.sgambitterra@unical.it

<sup>1</sup> Department of Mechanical, Energy and Management Engineering, University of Calabria, P. Bucci 44C, 87036 Rende, CS, Italy

[13–20] were analyzed. Many efforts were done to analyze the crack tip stress distribution and the size of phase transformation zone by numerical studies [21–26] which are mainly based on phenomenological approaches and on theory of plasticity, i.e., they use plasticity-like concepts to describe the effects of phase transformation mechanisms on the macroscopic response of NiTi alloys. Furthermore, analytical approaches [27–32], mainly based on modified linear elastic fracture mechanic (LEFM) theories, were also proposed in the last years.

Even though these methods represent useful design tools to simulate the macroscopic response of simple or complex SMA-based systems, special care should be taken when they are used to study the local effects in the proximity of high stress concentration regions where stress-induced phase transition mechanisms occur significantly affecting the crack tip stress distribution. Despite the increasing number of research activities on fracture and fatigue of NiTi alloys in recent years, much effort should be devoted for an effective understanding of the role of the phase transformations in the crack formation and propagation mechanisms and in the stress state generated at the crack tip.

Within this context, the development and application of full-field techniques to analyze the local transformation mechanisms near geometrical discontinuities and, in particular, in the crack tip region represents a highly challenging scientific goal. For this purpose, synchrotron X-ray microdiffraction (XRD) [8, 15, 18], infrared thermographic (IR) [11, 19], and digital image correlation (DIC) [16, 33, 34] techniques were recently applied, to better understand the mechanisms of phase transformation at the notch and/or crack tip proximity. In particular, a pseudoelastic NiTi alloy for medical applications was analyzed in [8] by using miniature compact-tension (CT) specimens, which were directly obtained from thin-walled tubes, similar to those used for manufacturing self-expanding stents. XRD microdiffraction investigations of fatigue pre-cracked specimens revealed that the crack tip local strain is due to both B2 (austenite) to B19' (martensite) transformation and to the subsequent loading of the martensitic phase. Strain and texture evolution near the crack tip of a martensitic NiTi alloy were analyzed in [15], by synchrotron X-ray experiments, after fatigue crack propagation in a compact-tension (CT) specimen; it was found that texture evolution is mainly due to detwinning phenomena, the main deformation mechanism in martensitic NiTi alloys. Both martensitic and austenitic alloys were analyzed in [18], by using miniaturized CT specimens after fatigue crack propagation, which revealed the presence of detwinned martensite at the crack tip of both martensitic and austenitic specimens. An austenitic NiTi alloy was analyzed in [16] by DIC analysis of thin edge cracked specimen, which

allowed direct measurement of the crack tip strain field related to stress-induced transformation. Furthermore, the stress intensity factor (SIF) evolution, as a function of the operating temperature, in a NiTi pseudoelastic alloy was investigated in [12] with a proper fitting procedure based on the William's series expansion [35], and thermal changes due to phase transformations in SMAs were investigated in [11]. Finally, nanoindentation technique, which was widely used to evaluate the mechanical properties of NiTi alloys [36], was proposed as an efficient and easy alternative method to identify near crack tip phase transformations in SMA alloys in [37].

These experimental investigations provide very useful information about the occurrence of crack tip transition mechanisms in NiTi alloys subjected to static and/or monotonic loads. However, more investigation should be carried out to better evaluate the effect of the temperature on the phase transformation zone near the crack tip.

To this aim, in the present work, the effect of the operating temperature on the crack tip transformation of a commercial pseudoelastic NiTi alloy (Type S, Memry, USA) was investigated by experimental approaches and analytical studies. In particular, single edge crack (SEC) specimens were analyzed for two different values of the testing temperature, i.e.,  $T = 298$  K and  $T = 338$  K, in the pseudoelastic regime of the alloy. The thermal-dependent phase transition mechanisms occurring at the crack tip region were studied by analyzing the strain data obtained from DIC investigations and the load vs. penetration response obtained from nanoindentation experiments performed near the crack tip. Finally, experimental results were compared with predictions of a recent analytical model [31].

Results revealed that nanoindentation technique is well suitable to identify the phase transformation zone near the crack tip, and good agreement with the analytical prediction was obtained; DIC is a powerful technique to evaluate the displacement fields whereas strain data result noisy with jagged contours. However, both the experimental techniques showed good capability in capturing the thermal effect on the phase transformation size near the crack tip.

## Materials and Methods

### Material

A commercial nickel–titanium sheet (thickness  $t = 0.5$  mm) with pseudoelastic properties at room temperature (50.8 at.% Ni–49.2 at.% Ti, Type S, Memry, Germany) was used in this investigation. Figure 1a shows the isothermal ( $T = 298$  K) stress–strain ( $\sigma$ – $\varepsilon$ ) response of the material obtained from a complete loading–unloading

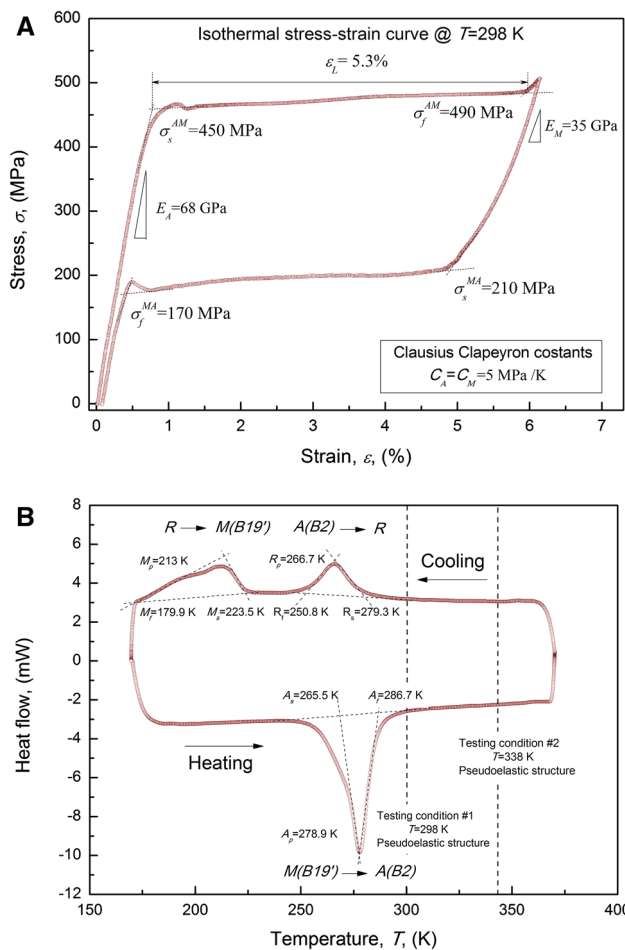


**Fig. 1** Thermo-mechanical properties of the investigated material: **a** loading–unloading isothermal stress–strain cycle (298 K) and **b** DSC thermograph with transformation temperatures

cycle up to a maximum deformation of about 6.2 %, corresponding to a complete stress-induced martensite transformation. The figure also reports the values of the main thermo-mechanical parameters of the alloy: transformation stresses ( $\sigma_s^{AM}$ ,  $\sigma_f^{AM}$ ,  $\sigma_s^{MA}$ , and  $\sigma_f^{MA}$ ), transformation strain ( $\epsilon_L$ ), Young's moduli of austenite and martensite ( $E_A$  and  $E_M$ ), and Clausius–Clapeyron constants ( $C_A$  and  $C_M$ ). Figure 1b shows the DSC thermogram of the alloy, which was measured in the temperature range between 173 and 373 K at a heating/cooling rate of 10 K/min. The figure clearly shows a two-stage phase transformation during cooling (B2-R-B19'), whereas there is no evidence of the R-phase transformation during heating (B19'-B2). The figure reports also the values of all transformation temperatures ( $M_s$ ,  $M_f$ ,  $A_s$ ,  $A_f$ ,  $R_s$ , and  $R_f$ ) as well as the latent heat of transformation.

Edge-notched tension specimens were cut from a commercial plate with electro discharge machining (EDM); a 0.1-mm EDM wire was used to machine the notch, as

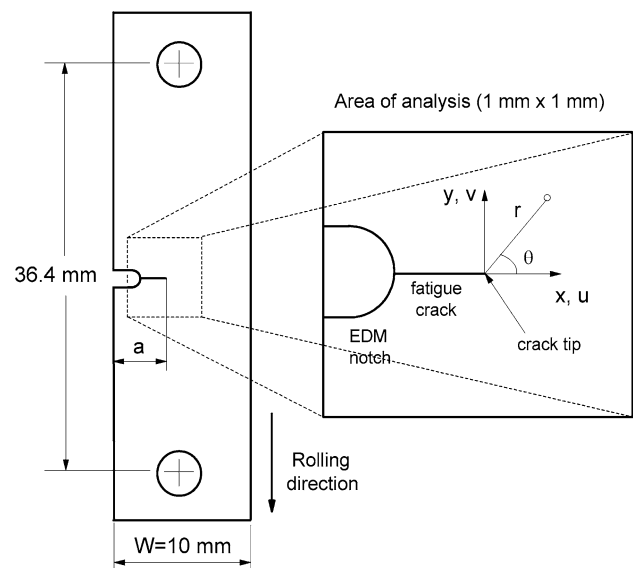


**Fig. 2** SEC specimen with a focus of the notch region

illustrated in Fig. 2. The specimen surface has been properly treated in order to provide a suitable speckle pattern for using DIC and to get a good surface roughness for the nanoindentation tests. In particular, grinding treatment with progressively finer silicon carbide papers (#400–#1000) and polishing with 1- $\mu$ m diamond compound was carried out; finally, the specimens were cleaned with acetone and dried in air.

Specimens were fatigue pre-cracked by using a servo hydraulic testing machine (Instron 8500), with a maximum load  $P_{max} = 100$  N ( $\sigma_{max} = P_{max}/Wt = 20$  MPa), at constant load ratio,  $R = \sigma_{min}/\sigma_{max}$ , of roughly zero, and at a rate of 5 Hz to initiate a crack from the EDM notch tip up to a length ratio ( $a/W$ ) in the range between 0.3 and 0.4 (see Fig. 2).

### Digital Image Correlation

Tensile load–unload measurements, at different operating temperature and with a maximum load  $P = 300$  N, corresponding to a maximum stress  $\sigma_{max} = P_{max}/Wt = 60$  MPa, were carried out in this investigation by using an electro-mechanical testing machine (MTS Criterion s42, USA).

A special system based on a Peltier cell and a thermocouple was used to set and control the temperature of the specimen during the tests.

A digital camera (Sony XCD- X910 model) with a resolution of 1280 by 960 pixels of 4.65  $\mu$ m was used to capture images throughout measurement tests. The focus of the images was performed using a Linos Photonics microscope objective with a 4 $\times$  magnification and a

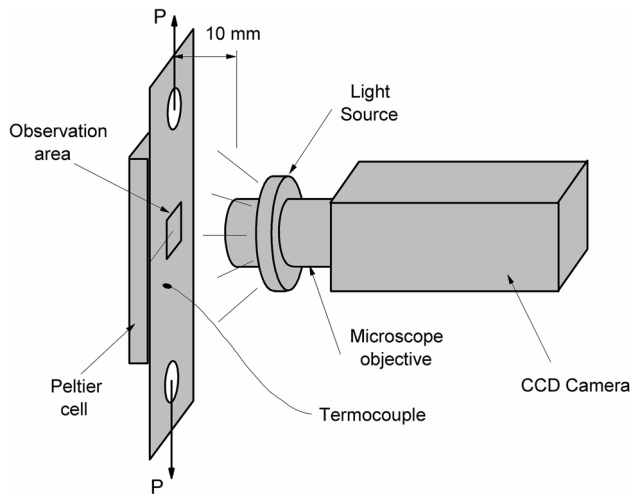


**Fig. 3** The experimental setup for DIC

numerical aperture of 0.1, which ensures, in conditions of correct illumination, a resolution of approximately  $2.5 \mu\text{m}$ , and therefore lower than the pixel size of the camera.

DIC was performed on images from each test carried at different operating temperatures using a commercially available image correlation software. The first image in the measurement cycle (at minimum load) was used as the reference image, and terms up to first-order displacement gradients were used in all correlations. DIC was used to obtain full-field displacements for each image throughout the cycle, and the correlations were performed using a subset size with a radius of 55 pixels and a spacing of 2 pixels between subset centers.

Finally, the whole experimental setup, see Fig. 3, including the testing machine, was placed on an anti-seismic platform to avoid measurement errors due to unavoidable vibrations.

### Nanoindentation

Temperature and load-controlled indentation tests were carried out by using a nanoindentation platform (CSM Instruments, Switzerland) equipped with a special properly developed frame (see Fig. 4a). In particular, a simple screw design system was used which allows to apply a fixed tensile load ( $P = 400 \text{ N}$ ), based on preliminary calibration data between crack mouth opening displacement and the applied load. A Peltier cell, together with a thermocouple, was used to set and control the temperature of the sample during nanoindentation tests. The experimental setup is shown in Fig. 4a. Nanoindentations were carried out by using a spherical tip, with a radius of  $20 \mu\text{m}$ , a maximum indentation load  $P = 400 \text{ mN}$ , and a dwell time equal to 10 s. These latter testing conditions were chosen based on some preliminary studies and on previous literature results

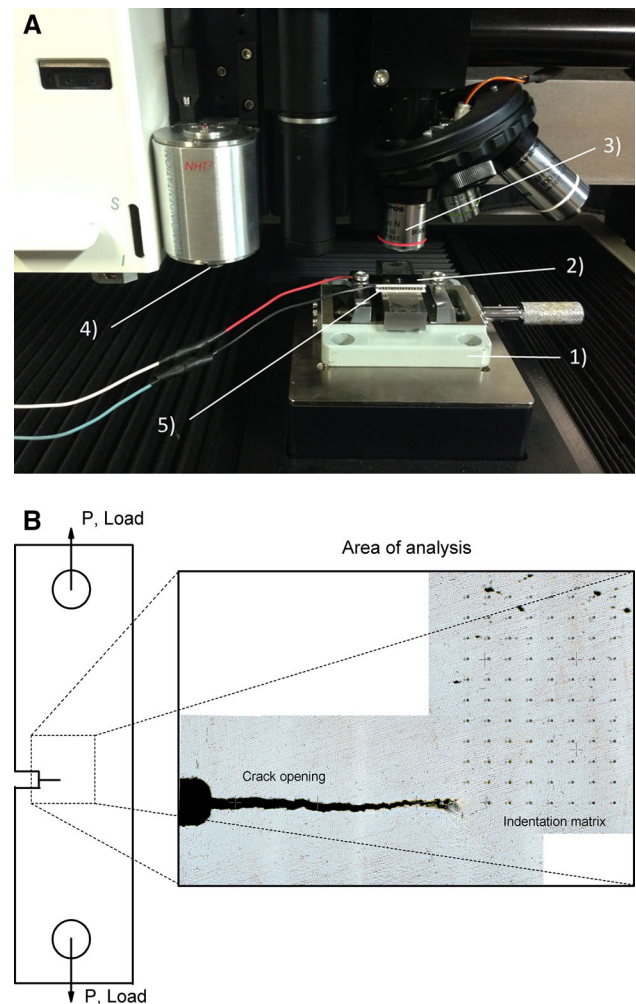


**Fig. 4** **a** The experimental setup for DIC, labeled in the figure: (1) system to apply the external load, (2) SEC specimen, (3) objective, (4) nanoindenter head, (5) peltier cell; **b** SEC specimen with micrograph of the crack tip region showing the indentation points

[38, 39]. In fact, the spherical tip was adopted instead of sharp tips (such as Berkovich, Vickers, etc.), to avoid high strain gradients, which promotes plastic deformations, dislocations and, consequently, inhibit the reversibility of phase transformation [38]. Furthermore, these testing conditions minimize the effects of crystallographic anisotropies [40] and of extremely localized surface microstructural changes, which could arise during mechanical polishing, due to the larger process zone compared to Berkovich tip and low indentation loads.

The indentation response at the crack tip region was analyzed by a matrix of 142 indentation points (see Fig. 4b), covering an area of  $1.7 \times 1.2 \text{ mm}^2$ , under an applied load  $P = 400 \text{ N}$  corresponding to a remote stress  $\sigma_0 = 80 \text{ MPa}$ . It is worth noting that only one side of the near crack tip region was analyzed in this study (see Fig. 4b).

### Analytical Modeling

A recent analytical model [31], which provides the extent of the transformation region, namely austenitic radius  $r_A$ , as a function of the thermo-mechanical loading condition of the alloy was used in this investigation in order to compare the predictions of the experimental results, obtained from DIC analysis and nanoindentation tests, with the analytical ones. In particular, Eq. 1 was used to calculate the austenitic radius for the SEC specimen, according to the iterative approach described in Ref. [31].

$$r_A = \frac{2K_{Ie}^2}{\pi\sigma_s^{AM}(\sigma_s^{AM} + \sigma_f^{AM})} + \left( \frac{2(E_A\epsilon_L - a_M^{-1}\sigma_f^{AM} + \sigma_s^{AM})}{(a_M^{-1} + 1 - 2\nu)(\sigma_s^{AM} + \sigma_f^{AM})} + 1 \right) r_M + \left( \frac{4(1 - \nu)K_{Ie}}{(a_M^{-1} + 1 - 2\nu)(\sigma_s^{AM} + \sigma_f^{AM})} \right) \sqrt{\frac{2r_M}{\pi}}, \tag{1}$$

where  $K_{Ie}$  is the effective stress intensity factor according to Ref. [31],  $\nu$  is the Poisson’s ratio,  $a_M$  is the Young’s modulus ratio ( $a_M = E_M/E_A$ ), and  $r_M$  is the martensitic radius, i.e., the extent of the fully transformed martensite at the very crack tip:

$$r_M = \left( \frac{(1 - \nu)K_{Ie}}{E_A\epsilon_L + (1 - 2\nu)\sigma_f^{AM} + \sigma_s^{AM}} \right)^2. \tag{2}$$

It is important to underline that both the equations were obtained considering a proper constraint factor, see Ref. [31], which takes into account the stress triaxiality effect at the crack tip (i.e., the effective transformation stress). In particular, as both the experimental techniques are based on surface measurements and due to the small thickness of the sample as well as the  $a/W$  ratio, plane stress conditions were assumed in this investigation and, in this way, the best comparison between the in-plane experimental measurements and the analytical predictions was obtained.

### Results

#### Preliminary Studies

Preliminary studies for the correlation analysis were carried out in order to set and optimize all the experimental parameters, i.e., spackle pattern, image resolution, and size of the investigation region. To this aim, full-field displacements were obtained from DIC, and contour plots of  $v$ -displacements (perpendicular to the crack line) and  $u$ -displacements (parallel to the crack line) were generated for each image recorded during the tests. Figure 5 shows  $v$  and  $u$ -displacement contour plots, corresponding to the

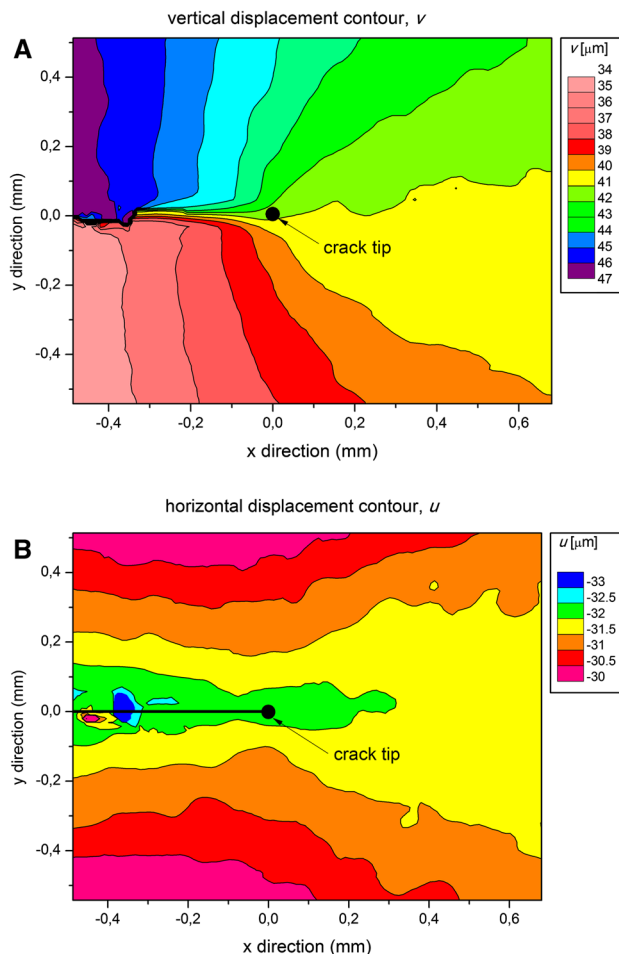


**Fig. 5** Calculated displacement fields near the crack tip from DIC: **a** vertical displacement ( $v$ ) contour plots; **b** horizontal displacement ( $u$ ) contour plots

peak load  $P = 400$  N, which were directly obtained from the DIC data.

In order to prove the feasibility of the technique in predicting the crack tip transformation region, the experimentally measured displacement contours were compared with a two parameters (stress intensity factor and T-stress) fracture mechanics solution proposed by Williams [35]. In particular, if the two in-plane rigid motion terms, rotation,  $A$ , and rigid translation perpendicular to the crack line,  $B$ , are introduced, then the equations for  $u$  and  $v$ -displacement contours can be written as follows:

$$u = \frac{K_I}{\mu} \sqrt{\frac{r}{2\pi}} \cos\left(\frac{\theta}{2}\right) \left[ \frac{1}{2}(k - 1) + \sin^2\left(\frac{\theta}{2}\right) \right] + \frac{1}{2\mu(1 + \nu)} Tr \cos(\theta) - Ar \sin(\theta) + B_u \tag{3}$$

$$v = \frac{K_I}{\mu} \sqrt{\frac{r}{2\pi}} \sin\left(\frac{\theta}{2}\right) \left[ \frac{1}{2}(k + 1) - \cos^2\left(\frac{\theta}{2}\right) \right] - \frac{1}{2\mu} \left( \frac{\nu}{1 + \nu} \right) Tr \sin(\theta) + Ar \cos(\theta) + B_v, \tag{4}$$

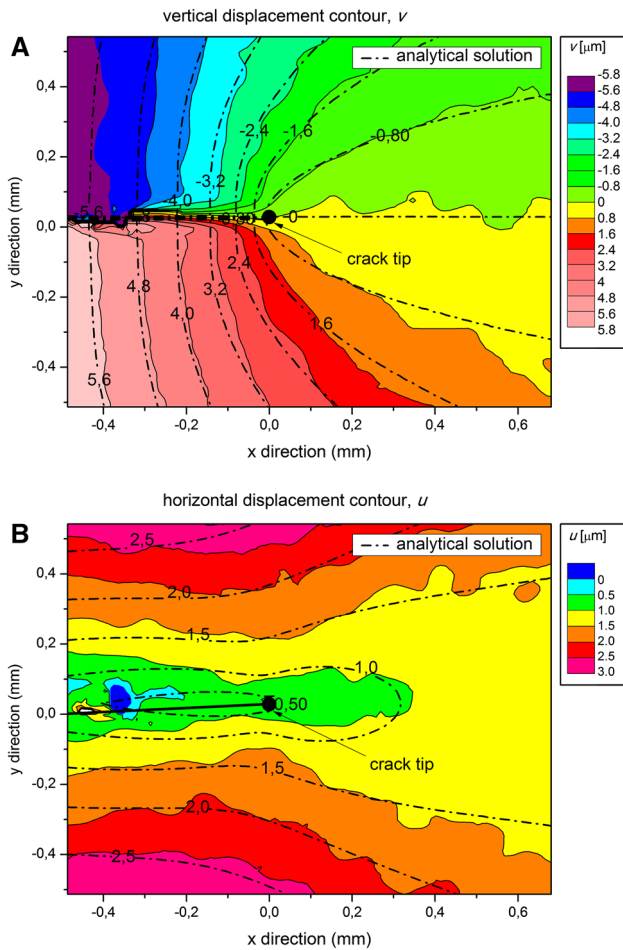


**Fig. 6** Comparison between the measured and the analytical displacement fields near the crack tip: **a** vertical displacement contour plots ( $v$ ); **b** horizontal displacement contour plots ( $u$ )

where  $K_I$  is the effective stress intensity factor,  $r$  and  $\theta$  are the polar coordinates of a system with the origin at the crack tip (see Fig. 2),  $\nu$  is the Poisson’s ratio,  $\mu$  is the shear modulus of elasticity, and  $k$ , for plane stress solution, is given by

$$k = \frac{3 - \nu}{1 + \nu}. \tag{5}$$

The comparison between the measured displacement contours and the analytical ones, after eliminating rigid body terms ( $A$  and  $B$ ), is reported in Fig. 6a, b, for the  $v$ -displacement and  $u$ -displacement contours, respectively, and results revealed very good agreement.

Displacement data were used to calculate the strain contours which allow to identify the crack tip transformation region, by a direct comparison with the stress–strain response of the material (see Fig. 1a), as illustrated in the following section.

Furthermore, preliminary ex situ indentation tests were carried out to study the nanoindentation response of the

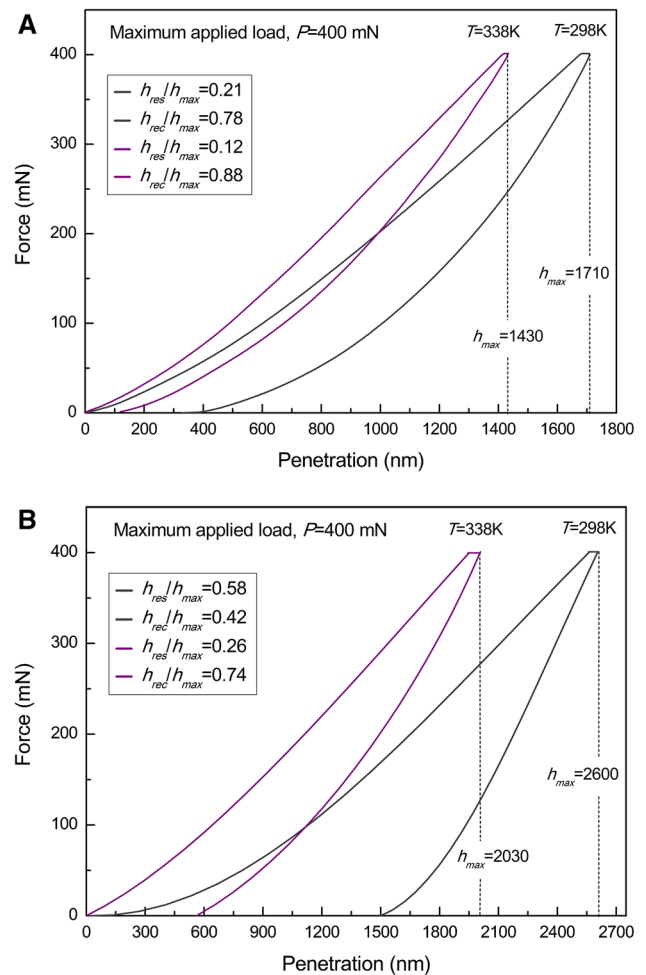


**Fig. 7** Indentation response as a function of the investigated testing temperature: **a** load–displacement curves for Type S alloy; **b** load–displacement curves for Type M alloy

two crystallographic phases of the alloy (martensite and austenite) as well as to identify suitable parameters to capture local phase transition mechanisms. In particular, isothermal stress-free indentation tests were carried out for the two values of the testing temperature ( $T = 298$  K and  $T = 338$  K) and two different materials were analyzed: i) the investigated Ni-rich austenitic alloy (Type S) and ii) a Ti-rich martensitic alloy (Type M, 49.8 at.% Ni–50.2 at.% Ti,  $A_f = 343$  K).

Figure 7 reports the obtained results in terms of load–penetration curves for type S and M alloys (Fig. 7a, b, respectively), and for the two investigated temperatures. Furthermore, the figures illustrate the measured values of the maximum depth ( $h_{max}$ ), residual depth ratio ( $h_{res}/h_{max}$ ), and the recovery depth ratio ( $h_{rec}/h_{max}$ ), which represent the parameters considered in this study, as also discussed in [37].

A direct comparison between the two materials shows very large differences, in terms of both  $h_{res}/h_{max}$  and

$h_{\text{rec}}/h_{\text{max}}$  ratios, which can be directly related to pseudoelasticity in austenitic alloys and pseudoplasticity in martensitic ones. In particular, Type S alloy shows a unusual indentation response with very large recovery depth if compared to Type M and also to common engineering alloys, i.e., with recovery depth ratios ( $h_{\text{rec}}/h_{\text{max}}$ ) equal to 0.78 at  $T = 298$  K and 0.9 at  $T = 338$  K, due to the reversible stress-induced transformations occurring during loading/unloading cycles. On the contrary, Type M alloy shows large residual depths, i.e., with recovery depth ratios ( $h_{\text{rec}}/h_{\text{max}}$ ) equal to 0.42 at  $T = 298$  K and 0.74 at  $T = 338$  K, due to pseudoplasticity associated with detwinning mechanisms occurring in the loading stage. In addition, as expected, Type M alloy shows much larger maximum depths if compared with Type S alloy, due to the detwinning phenomena, typical of a martensitic microstructures, which occur at lower stress values compared to the stress-induced martensite of the pseudoelastic alloys, according to the Clausius–Clapeyron law. Finally, both alloys show a marked effect of the testing temperature, i.e., an increase in temperature causes a decrease in the maximum depth and residual depth and an increase in the recovery depth, as a consequence of the temperature-dependent stress–strain response according to the Clausius–Clapeyron relation. Based on these preliminary results, the residual depth ( $h_{\text{res}}$ ) was identified as the most functional parameter to identify stress-induced phase transformations at the crack tip, as well as to analyze the effects of testing temperature.

### Crack Tip Transformation

Starting from the experimentally obtained displacement field, strain data were computed with the aim to evaluate the phase transformation zone near the crack tip, and the obtained results were compared with the analytical solution described in [31]. In particular, Fig. 8a, b reports the von Mises equivalent strain contours obtained at  $T = 298$  K (Fig. 8a) and  $T = 338$  K (Fig. 8b) together with the extent of the transformation region (black contours) obtained by the reference analytical model. These results are related to an external applied load  $P = 300$  N and a normalized crack length  $a/W = 0.3$  ( $K_0 = \sigma\sqrt{\pi a} = 6.8$  MPa $\sqrt{\text{m}}$ ). The experimental transformation contour can be estimated by the strain level  $\varepsilon_{\text{eq}} = 1$  %, which corresponds to the onset of stress-induced transformation, according to the stress–strain curve illustrated in Fig. 1a.

Nanoindentation tests at the crack tip region of the SEC specimen subjected to an applied load equal to  $P = 400$  N and a normalized crack length  $a/W = 0.42$  ( $K_0 = \sigma\sqrt{\pi a} = 7.8$  MPa $\sqrt{\text{m}}$ ) were carried out for the two different values of the testing temperature, equal to 298 K (Fig. 8c) and 338 K (Fig. 8d). Based on the preliminary

investigations, discussed in the previous section, the residual depth ( $h_{\text{res}}$ ) data, obtained from the indentation matrix, were analyzed, and the corresponding contour plots for  $T = 298$  K and  $T = 338$  K were computed. A comparison between Figs. 8c, d and 7 allows to identify the contours corresponding to full austenitic conditions, i.e., those corresponding to a residual depth close to 400 nm at  $T = 298$  K (Fig. 8c) and 200 nm at  $T = 338$  K (Fig. 8d). In addition, both figures show a similar trend of the residual depth ratio when moving from the outer austenitic region toward the crack tip, i.e., an increase of the residual depth is observed with maximum values close to 1000 nm at  $T = 298$  K and to 500 nm at  $T = 338$  K; it is important to point out that these values are very close to the residual depths obtained for the martensitic alloy at the same testing temperatures (see Fig. 7).

Even though a direct comparison between the results obtained from the two different experimental approaches cannot be done because of the different applied remote stress intensity factor ( $K_0$ ), Fig. 8 reports the transformation zone predicted by the two experimental methods together with the one analytically calculated [31]. In particular, DIC data revealed quite difference, in terms of shape and size, between the analytical and experimental transformation zone, for both the investigated thermal conditions, because the derivative procedure to calculate strain data gives strain plots generally noisier than displacement ones. On the contrary, very good agreements between the analytical predictions and the nanoindentation contours, corresponding to the fully austenitic structure, are observed. Furthermore, it is worth noting that both the experimental methods are able to capture the thermal effect on the phase transformation size according to the analytical predictions as well as to previous numerical [24] and experimental [12] studies. In particular, it is shown that an increase in temperature causes a decrease in the crack tip strain as a consequence of the increase in transformation stress, according to the Clausius–Clapeyron law.

### Conclusions

The effect of the testing temperature on crack tip transformation in a commercial pseudoelastic NiTi alloy was investigated by experiments and analytical model. Load-unload tensile tests, supported by DIC, and nanoindentation experiments were carried out on SEC specimens for two different values of the testing temperature in the pseudoelastic regime of the alloy, i.e.,  $T = 298$  K and  $T = 338$  K. In particular, the thermal-dependent phase transition mechanisms occurring at the crack tip region were studied by analyzing the strain data obtained from DIC investigations and the nanoindentation response performed near the

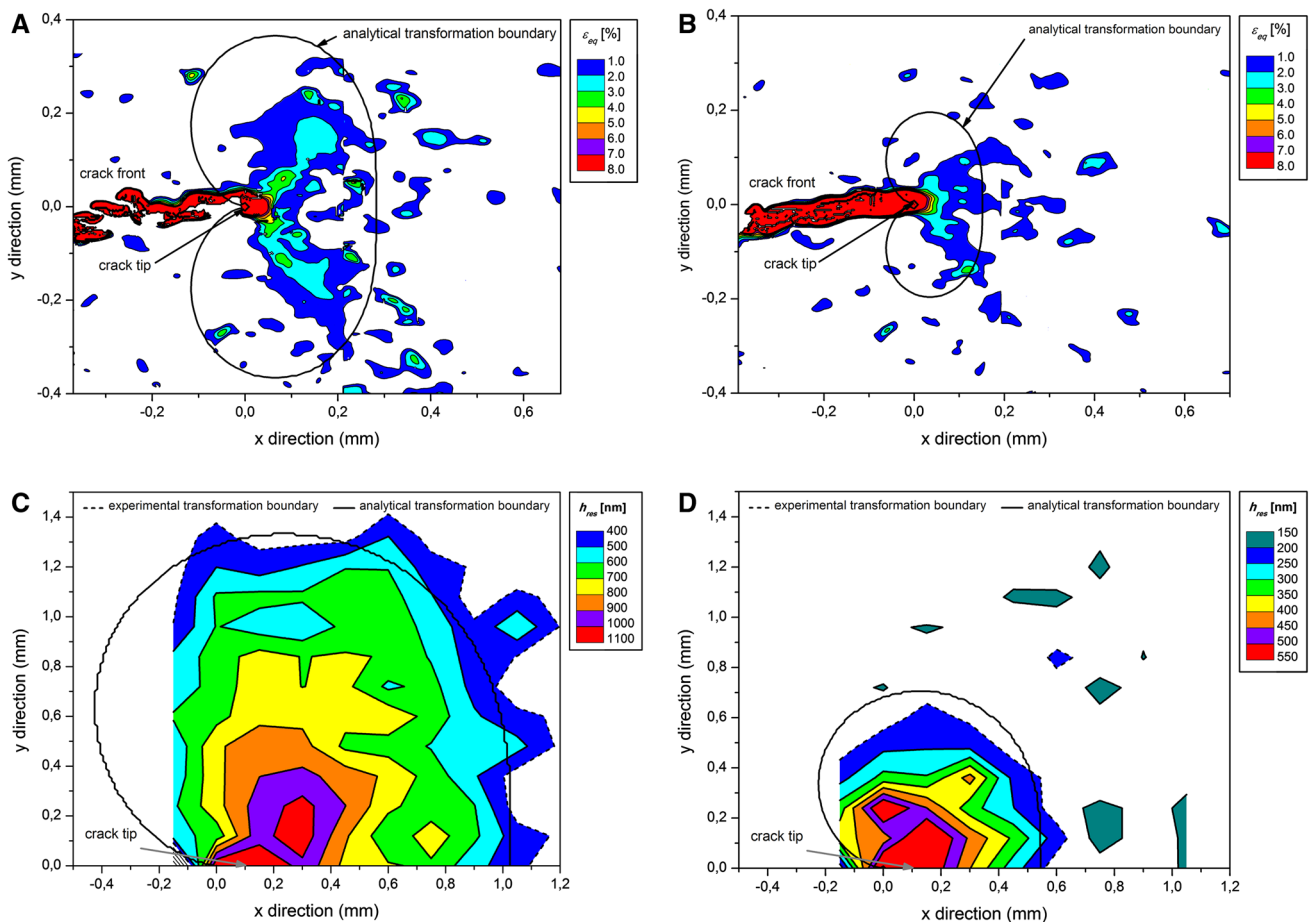


**Fig. 8** Experimentally measured crack tip transformation vs. analytical predictions [31] as a function of the testing temperature: contour plots of the crack tip strain obtained by DIC investigations at

$T = 298$  K (a) and  $T = 338$  K (b); contour plots of residual depths ( $h_{res}$ ) at the investigated crack tip region at  $T = 298$  K (c) and  $T = 338$  K (d)

crack tip. Finally, experimental results were compared with predictions of a recent analytical model. Results revealed that

- (1) an increase in temperature causes a decrease of the phase transformation zone as a consequence of the increase in transformation stress, according to the Clausius–Clapeyron law;
- (2) nanoindentation technique is well suitable to identify the phase transformation zone near the crack tip with good agreement with the analytical prediction;
- (3) DIC is a powerful technique to evaluate the displacement fields, however calculated strain data result noisy and revealed quite difference with the analytical predictions;
- (4) both the experimental techniques showed good capability in capturing the thermal effect on the phase transformation mechanisms near the crack tip.

**Acknowledgments** The authors wish to thank “MaTeRiA Laboratory” (University of Calabria), funded with “PON Ricerca e Competitività 2007/2013,” for providing equipment to perform nanoindentation experiments.

## References

1. Otsuka K, Wayman CM (1998) Shape memory materials. Cambridge University Press, Cambridge
2. Otsuka K, Ren X (2005) Physical metallurgy of Ti-Ni-based shape memory alloys. *Prog Mater Sci* 50:511–678
3. Duerig TW (1990) Engineering aspects of shape memory alloys. Butterworth-Heinemann, London
4. Duerig T, Pelton A, Stockel D (1999) An overview of nitinol medical applications. *Mater Sci Eng A* 273–275:149–160
5. Sawaguchi T, Kaustrater G, Yawny A, Wagner M, Eggeler G (2003) Crack initiation and propagation in 50.9 at. pct Ni-Ti pseudoelastic shape-memory wires in bending-rotation fatigue. *Metall Mater Trans A* 34:2847–2860
6. Robertson SW, Ritchie RO (2007) In vitro fatigue-crack growth and fracture toughness behavior of thin-walled superelastic nitinol tube for endovascular stents: a basis for defining the effect of crack-like defects. *Biomaterials* 28:700–709
7. Robertson SW, Ritchie RO (2008) A fracture mechanics based approach to fracture control in biomedical devices manufactured from superelastic nitinol tube. *J Biomed Mater Res Part B* 84:26–33
8. Robertson SW, Mehta A, Pelton AR, Ritchie RO (2007) Evolution of crack-tip transformation zones in superelastic nitinol subjected to in situ fatigue: a fracture mechanics and synchrotron X-ray microdiffraction analysis. *Acta Mater* 55:6198–6207



9. McKelvey AL, Ritchie RO (1999) Fatigue-crack propagation in Nitinol, a shape-memory and superelastic endovascular stent material. *J Biomed Mater Res* 47:301–308
10. McKelvey AL, Ritchie RO (2001) Fatigue-Crack growth behavior in the superelastic and shape-memory alloy nitinol. *Metall Mater Trans A* 32:731–743
11. Maletta C, Bruno L, Corigliano P, Crupi V, Guglielmino E (2014) Crack-tip thermal and mechanical hysteresis in shape memory alloys under fatigue loading. *Mater Sci Eng A* 616:281–287
12. Sgambitterra E, Bruno L, Maletta C (2014) Stress induced martensite at the crack tip in NiTi alloys during fatigue loading. *Frattura ed Integrità Strutturale* 30:167–173
13. Gall K, Yang N, Sehitoglu H, Chumlyakov YI (2001) Fracture of precipitated NiTi shape memory alloys. *Int J Fract* 109:189–207
14. Chen JH, Sun W, Wang GZ (2005) Investigation on the fracture behavior of shape memory alloy NiTi. *Metall Mater Trans A* 36:941–955
15. Daymond MR, Young ML, Almer JD, Dunand DC (2007) Strain and texture evolution during mechanical loading of a crack tip in martensitic shape-memory NiTi. *Acta Mater* 55:3929–3942
16. Daly S, Miller A, Ravichandran G, Bhattacharya K (2007) An experimental investigation of crack initiation in thin sheets of nitinol. *Acta Mater* 55:6322–6330
17. Gollerthan S, Herberg D, Baruj S, Eggeler G (2008) Compact tension testing of martensitic/pseudoplastic NiTi shape memory alloys. *Mater Sci Eng A* 481–482:156–159
18. Gollerthan S, Young ML, Baruj A, Frenzel J, Schmahl WW, Eggeler G (2009) Fracture mechanics and microstructure in NiTi shape memory alloys. *Acta Mater* 57:1015–1025
19. Gollerthan S, Young ML, Neuking K, Ramamurty U, Eggeler G (2009) Direct physical evidence for the back transformation of stress-induced martensite in the vicinity of cracks in pseudoelastic NiTi shape memory alloys. *Acta Mater* 57:5892–5897
20. Maletta C, Falvo A, Furguele F, Barbieri G, Brandizzi M (2009) Fracture behaviour of nickel–titanium laser welded joints. *J Mater Eng Perform* 18:569–574
21. Wang GZ (2007) Effect of martensite transformation on fracture behavior of shape memory alloy NiTi in a notched specimen. *Int J Fract* 146:93–104
22. Wang GZ, Xuan FZ, Tu ST, Wang ZD (2010) Effects of triaxial stress on martensite transformation, stress-strain and failure behavior in front of crack tips in shape memory alloy NiTi. *Mater Sci Eng A* 527:1529–1536
23. Falvo A, Furguele F, Leonardi A, Maletta C (2009) Stress induced martensitic transformation in the crack tip region of a NiTi alloy. *J Mater Eng Perform* 18:679–685
24. Maletta C, Sgambitterra E, Furguele F (2013) Crack tip stress distribution and stress intensity factor in shape memory alloys. *Fatigue Fract Eng Mater Struct* 36(9):903–912
25. Baxevanis T, Chemisky Y, Lagoudas DC (2012) Finite element analysis of the plane strain crack-tip mechanical fields in pseudoelastic shape memory alloys. *Smart Mater Struct* 21(9):094012. doi:10.1088/0964-1726/21/9/094012
26. Freed Y, Banks-Sills L (2001) Crack growth resistance of shape memory alloys by means of a cohesive zone model. *J Mech Phys Solids* 55:2157–2180
27. Birman V (1998) On mode I fracture of shape memory alloy plates. *Smart Mater Struct* 7:433–437
28. Lexcelent C, Thiebaud F (2008) Determination of the phase transformation zone at a crack tip in a shape memory alloy exhibiting asymmetry between tension and compression. *Scripta Mater* 59:321–323
29. Lexcelent C, Laydi MR, Taillebot V (2011) Analytical prediction of the phase transformation onset zone at a crack tip of a shape memory alloy exhibiting asymmetry between tension and compression. *Int J Fract* 169:1–13
30. Maletta C, Furguele F (2010) Analytical modeling of stress induced martensitic transformation in the crack tip region of nickeltitanium alloys. *Acta Mater* 58:92–101
31. Maletta C (2012) A novel fracture mechanics approach for shape memory alloys with trilinear stress-strain behavior. *Int J Fract* 177:39–51
32. Baxevanis T, Lagoudas DC (2012) A mode I fracture analysis of a center-cracked in NiTi shape memory alloy panel under plane stress. *Int J Fract* 175:151–166
33. Bewerse C, Gall KR, McFarland GJ, Zhu P, Brinson LC (2013) Local and global strains and strain ratios in shape memory alloys using digital image correlation. *Mater Sci Eng A* 568:134–142
34. Taillebot V, Lexcelent C, Vacher P (2012) About the transformation phase zones of shape memory alloys' fracture tests on single edge-cracked specimen. *Funct Mater Lett* 5(1):1250007. doi:10.1142/S1793604712500075
35. Eftis J, Subramonian N, Liebowitz H (1977) Crack border stress and displacement equations revisited. *Eng Fract Mech* 9:189–210
36. Gall K, Juntunen K, Maier HJ, Sehitoglu H, Chumlyakov YI (2001) Instrumented micro-indentation of NiTi shape memory alloys. *Acta Mater* 49:3205–3217
37. Sgambitterra E, Maletta C, Furguele F (2015) Temperature dependent local phase transformation in shape memory alloys by nanoindentation. *Scripta Mater* 101:64–67
38. Wood AJM, Clyne TW (2006) Measurement and modelling of the nanoindentation response of shape memory alloys. *Acta Mater* 54:5607–5615
39. Maletta C, Furguele F, Sgambitterra E, Callisti M, Mellor BG, Wood RJK (2012) Indentation response of a NiTi shape memory alloy: modeling and experiments. *Frattura ed Integrità Strutturale* 21:5–12
40. Pfetzing-Micklich J, Somsena C, Dlouhyb A, Begauc C, Hartmaier A, Wagner MF-X, Eggeler G (2013) On the crystallographic anisotropy of nanoindentation in pseudoelastic NiTi. *Acta Mater* 61(2):602–616